INTERNATIONAL JOURNAL OF AUTOMOTIVE AND MECHANICAL ENGINEERING
ISSN: 2229-8649 e-ISSN: 2180-1606
VOL. 20, ISSUE 4, 2023, 10917 – 10930
DOI: https://doi.org/10.15282/ijame.20.4.2023.09.0844

RESEARCH ARTICLE

Modeling and Tuning of Electronic Throttle Control System in Formula Student Car

K. Meetam[1], S. Gonsrang[1,2,*], C. Dechwayukul[1], W. Kaewapichai[3], P. Neranon[1], N. Vittayaphadung[1], and J. Auysakul[1]

[1]Department of Mechanical and Mechatronics Engineering, Faculty of Engineering, Prince of Songkla University, Hat Yai, Songkhla, 90110, Thailand
[2]Smart Industry Research Center, Faculty of Engineering, Prince of Songkla University, Hat Yai, Songkhla, 90110, Thailand
[3]Department of Computer Engineering, Faculty of Engineering, Prince of Songkla University, Hat Yai, Songkhla, 90110, Thailand

ABSTRACT - The Lookprabida formula student team uses an electronic throttle control (ETC) system in the racecar. Unfortunately, the ETC system cannot regulate the throttle valve to closely pursue angular setpoints. Thus, this paper endeavors to improve the response of the ETC system in racing cars. The ETC system is first examined using frequency response analysis. Parameter identification is carried out to obtain a mathematical model for the electronic throttle body. The Ziegler-Nichols' second method is then applied to preliminarily select the proportional integral derivative (PID) gains using MATLAB/Simulink®. Then, the ETC system fine-tuning on the experimental set is carried out. The final PID controller design results in a reduction in the settling time from 0.35 to 0.20 s, overshoot from 29.6 to 19.33%, and steady-state error from 2.00 to 0.22%. The racecar with the finally designed PID gains is tested on a training track; the root mean square error (RMSE) shows that the throttle valve approaches much closer to angular setpoints.

ARTICLE HISTORY
Received : 21st Apr. 2023
Revised : 08th Sept.2023
Accepted : 27th Nov. 2023
Published : 26th Dec. 2023

KEYWORDS
Formula student car,
Electronic throttle control,
Frequency response analysis,
ECU tuning,

1.0 INTRODUCTION

The study of the air intake system for the internal combustion engine is still ongoing [1], [2], [3], [4], [5]. An electronic throttle control (ETC) system is a common component of a car built with a spark-ignition engine. It adjusts the rate of the air intake to the engine's cylinders in terms of the pedal gas position and engine operation. Also, the electronic control unit (ECU) of the ETC system must define an air-fuel ratio that minimizes fuel consumption and tailpipe emission. The ECU control inputs a throttle plate and fuel injector into the signals from an airflow meter and fuel metering sensor, respectively. Thus, it is important to tune the parameters in the ECU.

Various techniques have been developed to control the throttle valve position. Proportional integral derivative *(PID)* control is the most commonly used due to its simplicity and ease of implementation. The *PID* gains in the throttle position produce the control signal by comparing the position of the throttle valve target with the actual position to minimize the angle error of the throttle plate [6]. Besides being used in passenger cars, low-cost throttle bodies controlled by *PI* controllers are employed in small motorcycles [7]. In this study, the adaptive backstepping controller is compared with the adaptive sliding mode backstepping controller. The simulation results show that the adaptive sliding mode backstepping controller has the ability to track the throttle position precisely during transient and steady-state conditions [8]. The author in [9] realizes an extended state observer (ESO) robust adaptive dynamic sliding mode (ADSM) for electronic throttle control. The simulation result reveals that the proposed controller achieves the lowest root mean square error (RMSE) in comparison to the adaptive sliding mode (ASM), conventional SM (CSM), and *PID* controls. However, the input used is a combination of trapezoid and sinusoidal waves, which do not reflect real-world driver commands. Fuzzy and immune feedback control algorithms are applied to improve the response performance of the *PID* electronic throttle control [10]. The simulation results reveal that both proposed methods can completely suppress the overshoot and improve the adjustment time compared to conventional *PID* and fuzzy *PID* control systems.

Among these methods, the *PID* control scheme is the most commonly adopted in modern cars because it is straightforward and robust [11]. The comprehensive review in the reference [11] mentions the use of a mathematic model in the control of the ETB. Parameterization of the ETB is fruitful for simulation and optimization in the throttle plate position control. However, the great challenge is to provide an accurate model, which is uneasy because of the use of nonlinear springs and airflow through the ETB. The ETC system includes a nonlinear compensator along with a *PID* controller. These two controllers cooperate to attain precise position control of a throttle valve even in the presence of a limp-home spring and friction [12], which cause nonlinear behavior of the throttle plate. It should be noted that the following friction components exist in the throttle body: Coulomb, static [13], Stribeck, viscous [14], and gearbox. Despite adding a compensator, differing sets of *PID* control gains are required for the different operating ranges of the throttle valve. Thus, it is crucial to identify the driving pattern and frequently used operation range of the throttle valve. This is so that the tuning of the ETC system can be more specific to the frequently used operation range.

***CORRESPONDING AUTHOR | S. Gonsrang** | ✉ sarawut.g@psu.ac.th

A mathematical model of the throttle body is an effective means of *PID* controller gain selection utilizing model-based design approaches. Thus, the modeling and parameter identification of the throttle body has been elaborated by the authors in [15]. Producing a high-fidelity throttle body model requires insight into all mechanical and electronic components, such as motor constants, spring constants, and preload torque. The researchers in [16] demonstrated the procedures for measuring dominant throttle body parameters and verifying by real-time control implementation. These parameters help to attain a highly accurate simulation of the throttle valve position, resulting in better control.

The Lookprabida formula student team of the Faculty of Engineering at Prince of Songkla University employed an electronic throttle body from BOSCH in the team's racing car. The used ECU was an aftermarket product. The design of the ETC system was based on FORMULA SAE® Rules 2023 [17]. The ETC system operated using closed-loop *PID* control. The *PID* gains were selected according to the general guidelines prepared by the ETC system supplier along with a published suggestion from other formula student teams. The values of *PID* gains in the ECU, such as proportional gain *P*, integral gain *I*, and derivative gain *D*, were 4, 0.137, and 30, respectively. However, the throttle valve position still lagged the setpoint. Consequently, the engine could not respond to the driver's request promptly. Many works have studied modeling, parameter identification, and the *PID* controller design of the ETC system and implemented it on a rapid control prototype or customized controller. However, to the authors' knowledge, no study has yet been published on practical ETC tuning.

This paper investigates engine control unit behaviors and demonstrates ETC tuning to improve the responses of the racing car's throttle valve. Section 2 presents a frequency response analysis for the realization of the throttle body's characteristics. Section 3 explains the parameter identification and derives a mathematical model of the throttle body in MATLAB/Simulink®. Section 4 shows the *PID* tuning procedure for time response improvement. Section 5 discusses and justifies the necessity for a performance study and parameter identification of the ETC system in terms of ECU tuning. A summary of this work is presented in Section 6.

The contribution of this paper is that it justifies parameter identification and a mathematical model for tuning a *PID* controller of the vehicle ECU. In addition, this study demonstrates operation-range identification, allowing the *PID* controller to be tailored to suit the frequently used working range. Furthermore, this paper proposes a *PID* gain design for throttle valve regulation, which requires fundamental engineering control knowledge. The experimental setup and Lookprabida's race car test results are also reported in this work. Figure 1 provides an overview of the research methodology used in this work.

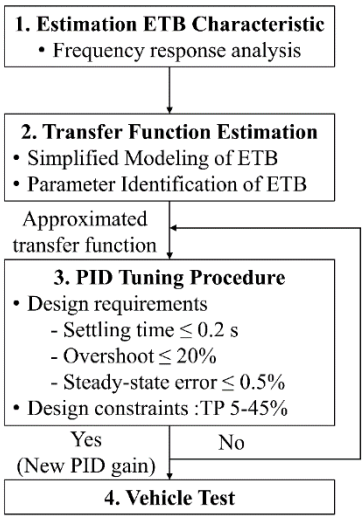

Figure 1. Research Methodology

2.0 FREQUENCY RESPONSE ANALYSIS OF ETC

An endurance test is the longest dynamic event of the formula student competition. This event evaluates the whole performance of the racecar and its drivers. The total score of the endurance event is greater than 40% of all dynamic events combined [17]. The formula student team has the edge to achieve a higher ranking in the competition if its racecar performs well in the endurance event. Thus, this work investigates ETC data during the endurance event to enhance the ETC response.

The endurance track shown in Figure 2 consists of various racing track layouts such as straight roads, constant turns, hairpin turns, slaloms, and chicanes. The racecar drivers need to be well-trained since they must finish the endurance circuit multiple times. The ETC system must also respond promptly to the throttle valve commands so that the drivers can adjust the traction force to the racing track.

Figure 3 depicts the control scheme of the throttle valve position in the formula student car from the Lookprabida team (Figure 4). Electronic throttle control (ETC) system consists of four components: an electronic control unit (ECU),

an electric throttle body (ETC), a throttle position sensor (TPS), and an accelerator pedal module. An accelerator pedal position transducer reads a gas pedal position and produces the throttle valve position setpoint. The ECU then adjusts the throttle valve position relating to the setpoint in a closed-loop control manner. Before implementing the tuning methods presented in this paper, the previously used *PID* gains of the ECU, such as a proportional gain P, integral gain I, and derivative gain, D, were 4, 0.137, and 30, respectively. These *PID* gains were selected according to the ETC manufacturer's instructions.

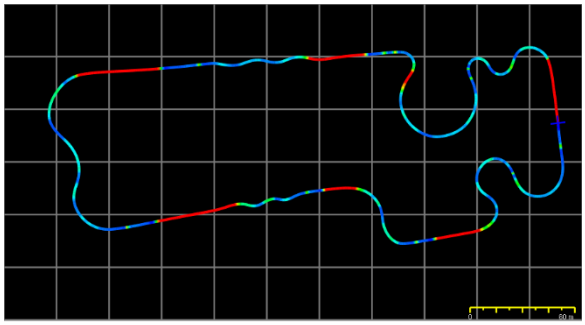

Figure 2. The layout of an 890-m endurance event on a 30-by-30-m grid. The track section where the throttle opens at 100% is indicated in red, while the blue line refers to the road section where the throttle position is at 0%

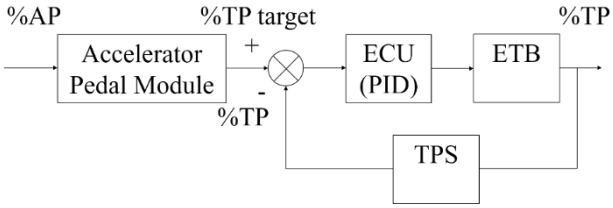

Figure 3. Electronic throttle control (ETC) system

Figure 4. The racecar of the Lookprabida team at Prince of Songkla University, Songkhla, Thailand

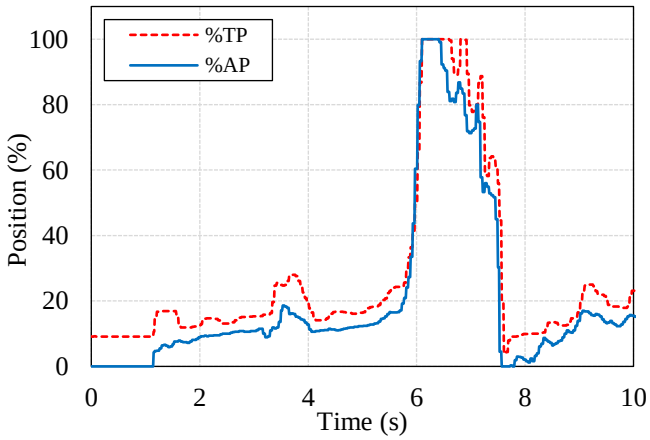

Figure 5. The gas pedal position sensor (%AP) and throttle position sensor (%TP) when ***P***, ***I***, and ***D*** gains are initially set at 4, 0.137, and 30, respectively

Figure 5 shows the throttle position in percentage terms (%TP) when the gas pedal is rapidly pressed and then released. The throttle position (%TP) lags behind the setpoint (%AP); in other words, the engine responds slowly to the driver's requests. This problem continued to exist at an endurance event in the Formula Student competition, causing a longer lap time. Thus, the *PID* controller in the ETC system needed to be redesigned.

To address this issue, it was first necessary to narrow the tuning range of the ETC system to analyze the operation of the throttle valve during an endurance event. The bar chart in Figure 6 (a) shows the usage proportion of the throttle valve in percentage terms at each throttle position range. Most of the throttle plate usage (77%) was between 5 and 45% of the throttle position (%TP). In addition, Figure 6 (b) presents the spectral analysis of the throttle valve operation, revealing that the throttle valve mostly operates at the frequency of one hertz.

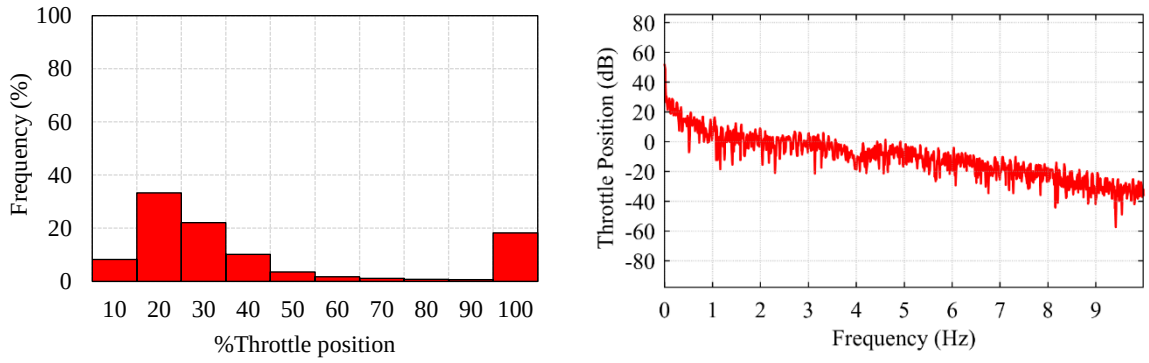

(a) (b)

Figure 6. Operating range of the throttle valve in an endurance scenario: (a) Histogram of the percentage throttle valve position, (b) Frequency response of the percentage throttle valve position

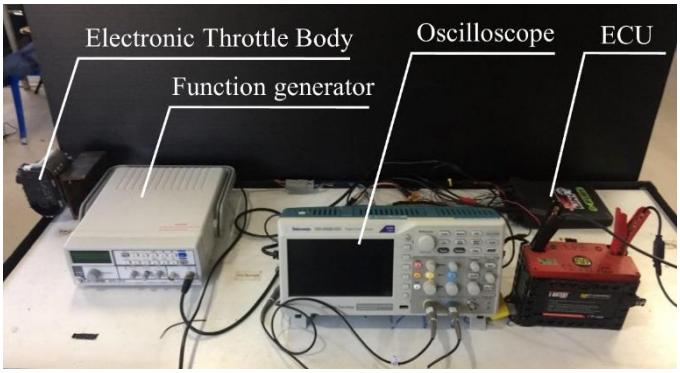

Figure 7. The experimental setup for the frequency response analysis, consists of four devices: an electronic throttle body, an electronic control unit (ECU), a function generator, and an oscilloscope

After that, this study carried out a frequency response analysis to further realize the behaviors of the ETC system. Figure 7 shows the experimental setup for the frequency response analysis. According to the analysis results from the last paragraph, the sinusoidal excitation of the frequency-response test was in the range of 0.5-10 Hz with a 0.5 Hz increment.

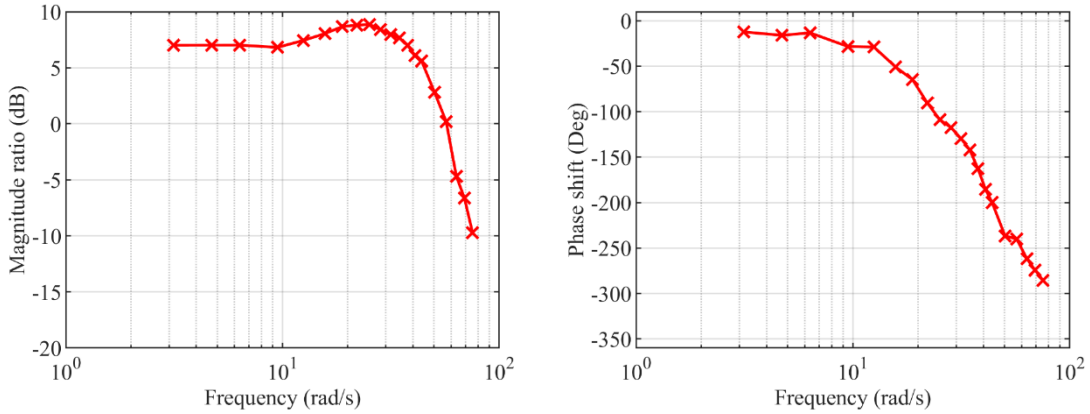

(a) (b)

Figure 8. Bode plots of the throttle position control system: the ETC system, under excitement with a sinusoidal wave at frequencies ranging from 0.5 to 10 Hz, with an increment of 0.5 Hz

Figure 8 (a) and 8 (b) show that the ETC system behaves as a fourth-order lag system in the testing frequency range. These results agree with the data from actual driving in Figure 5 that the closed-loop throttle valve control system follows the angle setpoints with considerable errors. The magnitude ratio is constant in the frequency, ranging from 1 to 10 rad/s, and the phase lag gradually increases to 27 degrees. The phase lag subsequently increases and reaches 180 degrees at a frequency of 40 rad/s.

An open-loop transfer function of the plant under consideration can be obtained by further inspecting the results from the frequency response analysis. However, this is not the case here since the ETC system is an off-the-shelf product, which is manufactured to work in a closed loop. Therefore, parameter identification was carried out to obtain essential information about the ETC system, as presented in the subsequent section.

3.0 TRANSFER FUNCTION ESTIMATION

3.1 Simplified Modeling of the Throttle Body

The throttle body under study (Figure 9) was BOSCH, order number 0280750148. This section explores the technical specifications of the electronic throttle body.

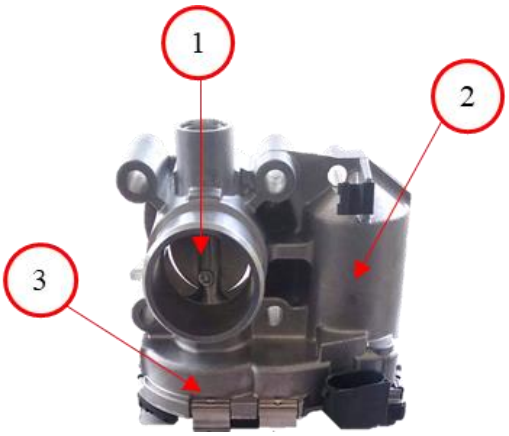

Figure 9. Bosch electronic throttle body, comprising three components: (1) a throttle valve, (2) a brushless DC motor, and (3) a throttle position sensor

- *Throttle valve*

A brushless DC (BLDC) motor is an actuator that drives the throttle valve via a 20:1 gearbox. The throttle plate swings between 0 - 90 degrees in the throttle body owing to mechanical stoppers. A returning spring pulls the throttle plate back into a closed position when the engine stops. In the case of system failure, a preloaded spring keeps the throttle plate at the default position [18], also called the limp-home spring position [19].

- *BLDC motor*

The ECU controls the BLDC motor pertaining to the signals from the accelerator pedal position sensor and the rotary potentiometer. Table 1 shows the relationship between the voltage read by the throttle position sensor (TPS) and the position of the throttle valve.

- *Throttle position sensor*

The throttle position sensor (TPS) is a rotary potentiometer, generating a voltage feedback ranging from 0 to 5 V with a ±0.2 V error. The throttle plate is completely closed: TPS = 0 degrees when the throttle position sensor reads 0.45 V. The voltage of the position sensor becomes 4.73 V when the throttle plate is fully open: TPS = 90 degrees.

Table 1. Relationship between the throttle position sensor (TPS) and throttle valve position

Throttle plate position	TPS (V)	Throttle valve position	
		(%)	(degree)
Upper stopper	4.73	100	90
Default position	0.88	10	9
Lower stopper	0.45	0	0

Figure 10 shows a simplified schematic of the throttle body, consisting of an electric motor and a throttle valve. The armature current flowing through the circuit of the DC motor obeys the following equation:

$$L_a \frac{di_a(t)}{dt} + R_a i_a(t) + K_b \dot{\theta}_m(t) = v_a(t) \tag{1}$$

where R_a is the armature resistance; L_a is the armature inductance; K_b is the constant of an electromagnetic force; v_a is the motor-supplied voltage; i_a is the armature current; θ_m is the angular motor position; θ_L is the angular position of the throttle plate, and N is the reduction gear ratio. It should be noted that the motor angular position equals the throttle plate position times the reduction gear ratio: $\theta_m = N\theta_L$.

According to Figure 10, the following expression describes the torque balance on the mechanism side:

$$(J_m N^2 + J_L)\frac{\left(d^2\theta_L(t)\right)}{dt^2} + (B_m N^2 + B_L)\frac{d\theta_L(t)}{dt} + K_s\theta_L(t) + T_{PL} + T_f = NK_m i_a(t) \tag{2}$$

where K_m is the torque constant; J_m is the motor's inertia; J_L is the throttle plate's inertia; B_m the motor viscous damping coefficient; B_L the throttle plate viscous damping coefficient; K_s is the returning-spring stiffness; T_{PL} is the spring-preloaded torque; and T_f refers to friction against the movement of the throttle plate. The next section explains the parameter identification method used to obtain the constants of Equations (1) and (2).

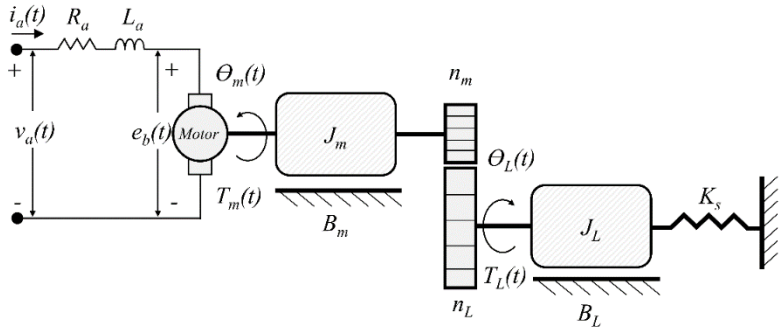

Figure 10. Schematic of the electronic throttle body

3.2 Parameter Identification of the Throttle Body

This work follows the parameter identification of the electric throttle body from BOSCH presented in [15] and [16]. A low pass filter is used to reduce signal noise, easing the parameter approximations from the graphs. The results from the parameter identification are explained in this section.

- Motor Resistance Test

The first test begins by halting the throttle plate in a closing position to maintain the electromagnetic force at zero. A constant voltage is then supplied to the motor. The data logger records the armature current from the start until steady-state conditions are fully developed. This test is repeated at differing supply voltages to obtain enough data points for resistance calculation.

Figure 11 shows the variation of the current when the applied voltage varies from zero to 3.4 V. According to Equation (1), the slope of the linear approximation in Figure 11 equals one over the armature resistance. Thus, the resistance of the motor, R_m, is about 1.513 Ω.

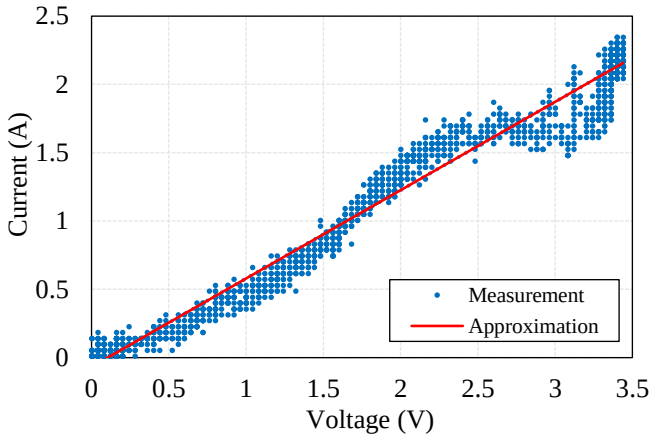

Figure 11. The values of the armature currents at different voltages

- *Motor Inductance Test*

The throttle plate is prevented from moving to keep the back-emf at zero. The motor then receives a unit step voltage from the supply.

The armature current profile shown in Figure 12 depicts the motor current during the motor inductance test. By equating the motor angular speed to zero, the solution to Equation (1) becomes

$$i_a(t) = \frac{v_a}{R_t}\left(1 - e^{-t/\tau}\right), \qquad t \geq 0 \tag{3}$$

The resistance R_t in the above equation combines the resistance of the motor circuit, sensor, and wiring harness. The parameter τ in Equation (3) is the electrical time constant of the motor, representing the multiplication between parameters L_a and R_t.

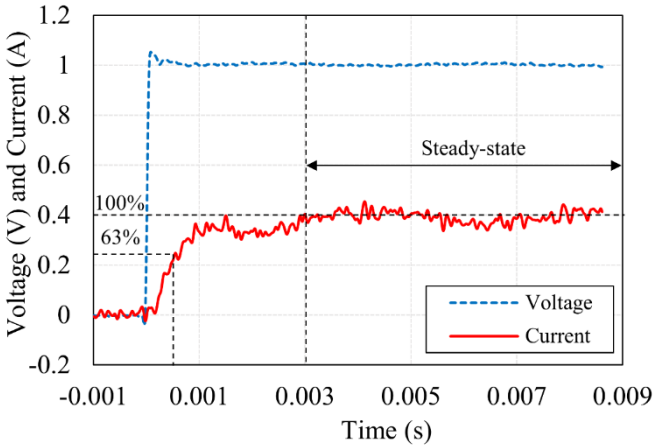

Figure 12. The voltage profile against the armature current in the inductance test

As can be observed from Figure 12, the steady-state motor current is approximately 0.368 A, when the supplied voltage is 1.005 V. The ratio between v_a and i_a is the resistance R_t, which equals 12.731 Ω. The time constant τ is the duration the armature current takes to develop from 0 to 63% of its final value; the constant τ in this study is around 0.54 ms. The motor inductance L_a is estimated at 1.475 mH.

- *Back Electromotive Force Test*

The measurement of constants K_m and K_b requires the throttle plate to be fully open at the start. The throttle plate is then released, and the returning spring pulls the plate back into a closing position.

The back-emf voltage and angular velocity in Figure 13 are considered at $t = 0.2$ s when the angular speed appears to be almost steady. Thus, the armature current and its time derivative approach zero. The back-emf voltage, denoted by e_b, becomes directly proportional to the plate's angular velocity, denoted by ω_L. According to Equation (1), the ratio of e_b to ω_L equals the back-emf constant $\overline{K}_b$:

$$\overline{K}_b = \frac{v_a(t)}{\dot{\theta}_m(t)} = \frac{e_b(t)}{\omega_L} \tag{4}$$

where the unit of $\overline{K}_b$ is V·s/rad. In this study, the values of e_b and ω_L are around 5.12 V and 13.10 rad/s, respectively, at $t = 0.2$ s (Figure 13). As a result, the back-emf constant is about 0.391 V·s/rad. The value of the motor torque constant, denoted by $\overline{K}_m$, resembles that of $\overline{K}_b$; but the unit of $\overline{K}_m$ is N·m/A instead. Accounting for a gear reduction ratio of 20.68, the estimates of the final back-emf constant K_b and the final torque constant K_m are 0.0189 V·s/rad and 0.0189 N·m/A, respectively.

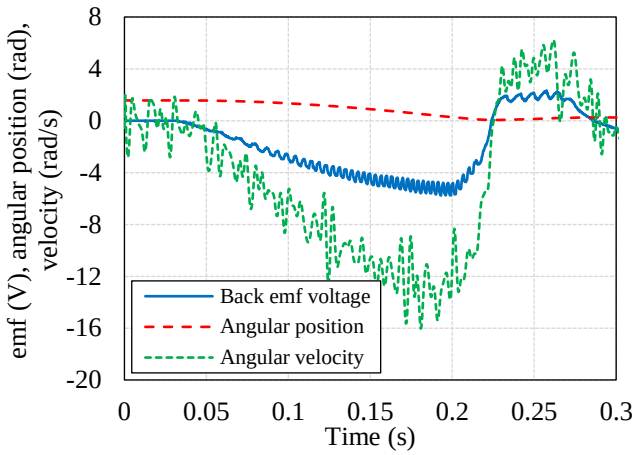

Figure 13. The back-emf, angular position, and angular velocity in the back electromotive force test

- *Static Load Test*

The static load test is used to obtain the following parameters: friction torque (T_f), preloaded torque (T_{PL}), and spring constant (K_s). This test starts by gradually increasing the supply voltage to the motor. After setting the throttle plate to a fully open position, the provided voltage decreases steadily until the plate returns to a completely closed position.

According to Equation (2), the load torque, T_L, is a combination of the torque from the angular spring, preloaded torque, T_{PL}, and friction torque, T_f:

$$T_L(t) = K_s\theta_L(t) + T_{PL} \pm T_f \tag{5}$$

Figure 14 reveals the net torque produced by the motor at each opening and closing angle of the throttle plate. The load torque is the sum of the spring, preloaded, and friction torques. However, torque T_L equals the sum of the spring torque and preloaded torque deducted by the friction torque.

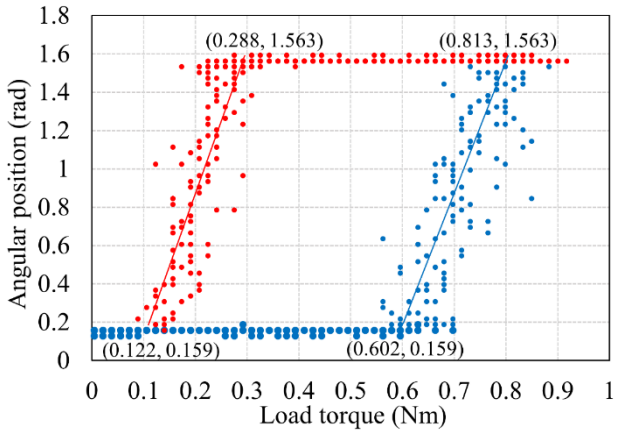

Figure 14. The static load test showing the torque profile during the throttle plate opening (blue line) and closing (red line)

According to the blue dots in Figure 14, the motor torque is around 0.602 N·m before the valve opens wider than 0.159 radians; the total load torque at this moment is the sum of T_{PL} and T_f. Furthermore, the motor produces a torque of approximately 0.122 N·m when the valve approaches 0.159 radians again; the load torque equals the torque T_{PL} deducted by T_f. Thus, by solving the system of equations, T_{PL} and T_f can be estimated at 0.362 and 0.239 N·m, respectively. As can be observed by the blue dots in Figure 14, the throttle valve requires around 0.211 N·m more to tilt from 0.159 to 1.563 radians. Therefore, the stiffness K_s is approximately 0.150 N·m/rad.

- *Viscous Frictional Coefficient Test*

This experiment analyzes the viscous friction coefficients of the motor by inspecting the current response to a step voltage. An infrared sensor module (HW-201) observes the angular velocity of the motor shaft. This procedure is repeated at differing step voltages ranging from 2 to 12 V, with an increment of 2 V.

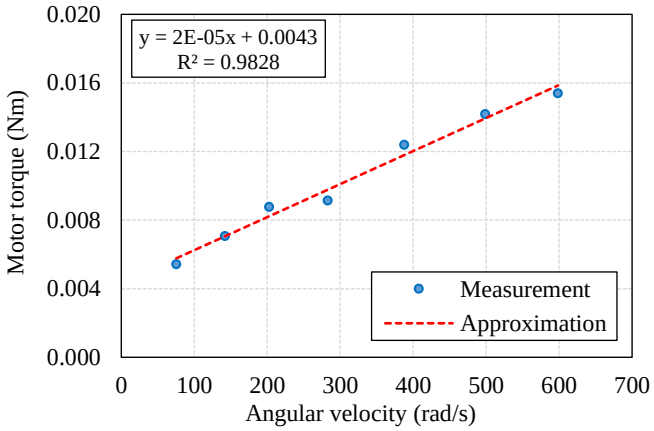

Figure 15. The motor torque versus the angular velocity in the viscous frictional coefficient test

Figure 15 presents the motor torque at differing motor speeds. The motor torque, T_m, equals the motor current times the constant K_m, the value of which is 0.0189 N·m/A. In addition, the BLDC motor and throttle valve are disconnected. According to Equation (2), the relationship between the motor torque and motor speed can be expressed as:

$$T_m(t) = B_m \frac{d\theta_m(t)}{dt} \tag{6}$$

The slope of the dashed graph in Figure 15 equals the viscous coefficient of the motor, B_m, which is around 0.00002 N·m·s/rad. Thus, the equivalent viscous friction coefficient of the throttle body B_{eq} in Equation (2) becomes approximately 0.0085 N·m·s/rad when the constant B_L is neglected [16].

- *Moment of Inertia Test*

The throttle plate is fully open at the start and then released and pulled back to a closed position by the returning spring. The angular position and the back-emf, e_b, are recorded during the test. Since the armature current, i_a, approaches zero during testing, the torque balance Equation (2) becomes

$$J_{eq} = -\frac{B_{eq}\frac{d\theta_L(t)}{dt} + K_s\theta_L(t) + T_{PL} + T_f}{\frac{d^2\theta_L(t)}{dt^2}} \tag{7}$$

The equivalent inertia, J_{eq}, in Equation (7) equals $N^2J_m + J_L$. The division of e_b with $\bar{K}_b$ is an estimate of the time derivative of θ_L. Furthermore, a finite change in the angular speed over a small-time interval approximates the second-order derivative of θ_L to time: $\frac{d^2\theta}{dt^2} \approx \Delta\omega_L/\Delta t$. T_{PL} and T_f are constant. Thus, the average moment of inertia is around 0.0012 kg·m^2, calculated from the period of 0.04 to 0.16 s in Figure 16. Table 2 provides the parameters required for formulating the mathematical model of the electric throttle body. According to Equations (1) and (2), and the parameters in Table 2, the transfer function of the electric throttle body in Figure 10 is as follows:

$$G(s) = \frac{3.10 \times 10^4}{s^3 + 113.8s^2 + 2941s + 2.38 \times 10^4} \tag{8}$$

The transfer function (8) provides insight into the characteristics and eases to tune the ETC system in the vehicle. The utilization of the transfer function (8) is demonstrated in the next section.

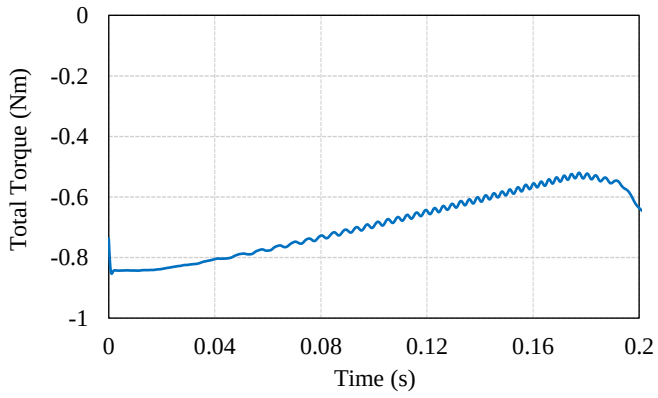

Figure 16. The result of the total torque in the moment of inertia test

Table 2. Technical parameters of the BOSCH throttle body derived using parameter identification

Symbols	Values	Units	Symbols	Values	Units
R_a	1.513	Ω	T_{PL}	0.362	N·m
L_a	1.475	mH	T_f	0.239	N·m
K_b	0.0189	V·s/rad	N	20.68	-
K_m	0.0189	N·m/A	J_{eq}	0.0012	Kg·m^2
J_m	0.0001	Kg·m^2	B_{eq}	0.0085	N·m·s/rad
J_L	0.0012	Kg·m^2	K_s	0.150	N·m/rad
B_m	0.00002	N·m·s/rad	B_L	0	N·m·s/rad

4.0 ETC SYSTEM TUNING AND RESULTS

4.1 Design Requirements

The major challenge of this work was that the throttle position (%TP) differs from the setpoint (%AP) by around 10 to 20% as mentioned in Section 3 (Figure 5). The lag response of the ETC system was expected to improve by retuning the *PID* gains of the ECU. As mentioned in Section 3, the old set of *PID* gains resulted in a high overshoot of almost 30%, a long settling time of 0.35 s, and a fair steady-state error of 2%. The new *PID* controller design had to enhance the response of the ETC system to the driver by achieving the following goals: (a) a settling time shorter than 0.2 s, (b) an overshoot smaller than 20%, and (c) a steady-state error below 0.5% of the fully developed magnitude.

The waveform for testing the ETC system was trapezoidal, with the magnitude fraction ranging from 5 to 45% at the frequency of 1 Hz. The trapezoidal wave train was chosen because this waveform resembled the signal from the gas pedal.

4.2 PID Tuning Procedure

Figure 17 reveals that the transfer function (8) can closely simulate the behavior of the actual ETC system (Figure 7). Thus, this transfer function can be used in the preliminary design of the *PID* controller. The *PID* tuning process in this work consists of two steps, the first being preliminary *PID* tuning based on a mathematic model (8) under a MATLAB/Simulink® environment. The preliminary *PID* gains are then implemented on the experimental ETC set for fine-tuning. The development of *PID* tuning is reported in this section.

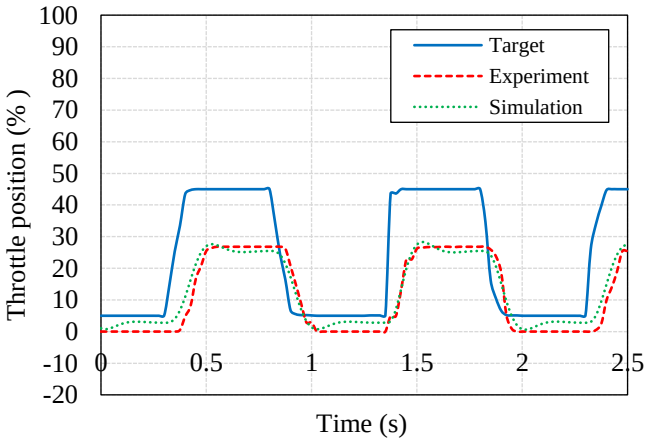

Figure 17. Comparison of the percentage throttle position between the real-time control and simulation results

It should be noted that the transfer function of the ETC system can be obtained using a frequency-response analysis as well. According to the frequency response analysis in Section 0, the ETC system is a fourth-order lag system. Nonetheless, the expression (8) is a third-order transfer function. This discrepancy may arise because of nonlinearities in the electric throttle body due to a limp-home spring and Coulomb friction [11]. Also, the devices that may cause the system order difference are the pulse-width modulator (PWM) and the angular position transducer in the ETC system. Thus, this paper excludes the ETC's transfer function via the frequency analysis from *PID* gain consideration.

In the preliminary *PID* gain tuning, c was adopted owing to its simplicity and wide adaptation. The preliminary *PID* gains using the Ziegler-Nichols second method were as follows: $P = 6$, $I = 103.59$, and $D = 0.088$. Figure 18 shows the simulation on MATLAB/Simulink® when the new *PID* gains were implemented in the ETC system. The throttle plate operation almost satisfied the design goals: the settling time was 0.35 s; the overshoot was 18.27%; and the steady-state error was 0.22%.

Nevertheless, the throttle valve of the experimental set (Figure 7) oscillated after implementing the preliminary set of *PID* gains and failed to approach the angle setpoint. As stated earlier, a limp-home spring and Coulomb friction might be

the reason for the discrepancy between the plant simulation and the ETC testing set. The authors in [20] suggest using a nonlinear spring and friction compensator to tackle this nonlinearity problem. Unfortunately, the use of a compensator is infeasible in this work because the ECU (Link G4 Fury) is an aftermarket part. Thus, adjusting the *PID* gains is the only option.

The *PID* fine-tuning was subsequently carried out based on the preliminary *PID* gains. The proportional gain was initially set to 6.0, while the integral and the derivative gain were set to zero in the experimental setup (Figure 7). However, the throttle plate swung harshly. Thus, the gain *P* was reduced to 5.5 and 4.0, respectively, to decrease oscillation. Nevertheless, the magnitude of the throttle valve's oscillation was still unacceptable, as shown in Figure 19. Furthermore, the smaller the proportional gain, the worse the rise time became. Thus, the gain *P* was fixed to 5.5 to maintain a fast rise time. Instead of reducing the proportional gain, the derivative gain was then selected to suppress oscillation.

The derivative gain was increased to 30 so the overshoot and settling time were reduced to 9.52% and 0.22 s, respectively. Gain *D* was then further increased to 40; the overshoot and the settling time correspondingly decreased to 3.58% and 0.18 s, respectively. However, the derivative gain should not be larger than 40 to refrain from extending the settling period of the ETC system.

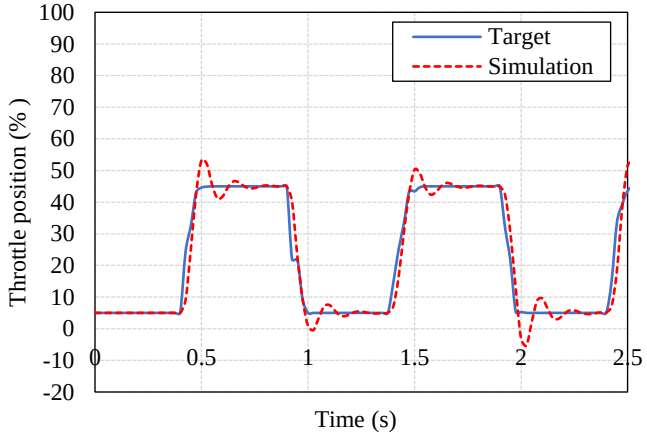

Figure 18. Comparison of the percentage throttle position between the target and simulation results after *PID* tuning in MATLAB/Simulink®; the controller gains *P*, *I*, and *D* were 6.06, 103.59, and 0.088, respectively

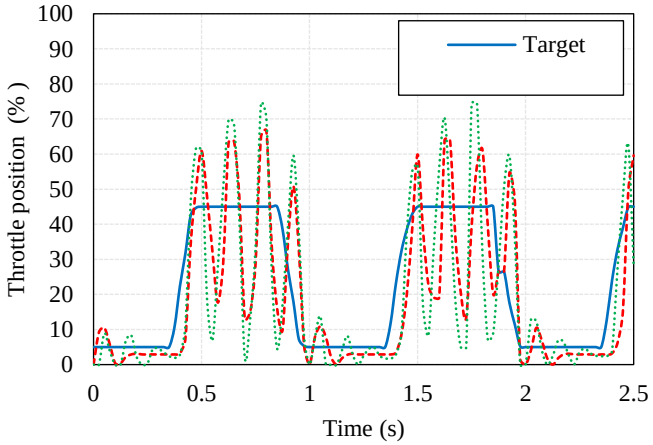

Figure 19. Comparison of the throttle position between the target and results after *PID* tuning in the experimental setup

After tuning gains *P* to 5.5 and *D* to 40, the steady-state error remained at 6.89%. Thus, the integral gain could be a small figure to make the steady-state error gradually die away. Gain *I* was initially set to 0.013 and the steady-state error was reduced to 1.56%. However, the error was still larger than the set value of 0.5%. Then, the gain *I* in this work was stepped up to the initial value of 0.137; the steady-state error was reduced to 0.22% as a result. Nevertheless, the overshoot ascended from 3.58% to 19.33%, thus gain *I* should not be greater than 0.137 to restrain the overshoot of the ETC system from exceeding the set value of 20%.

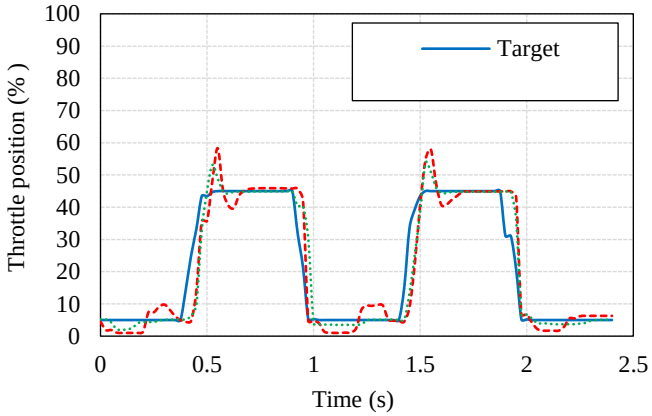

Figure 20. Comparison of the throttle position between the target and result after performing *PID* selection on the experimental set

The response of the ETC system, when $P = 5.5$, $I = 0.137$, and $D = 40$, can be seen in Figure 20. Even though the overshoot in the throttle plate was seemingly severe, it still met the design requirements set in the previous subsection. Also, the steady-state error and the settling time were reduced to 0.22% and 0.2 s, respectively, as shown in Table 3. The second set of *PID* gains was implemented in the racecar. The throttle plate behaviors are reported in the following subsection.

Table 3. The comparison between the ETC system response with the initial tuning and with the new tuning

Parameter requirements	*PID* gains	
	Initial tuning (P = 4, I = 0.137, D = 30)	New tuning (P = 5.5, I = 0.137, D = 40.)
Overshoot	29.6%	19.33%
Steady-state error	2%	0.22%
Settling time	0.35 s	

4.3 Vehicle Test Results

The formula student car with the new *PID* gains was tested on a proving ground, which included some low-speed corners, short-straight sections, and one slalom.

Figure 21 and Figure 22 show the throttle positions that closely approach the target. The magnitudes of the difference between the throttle valve positions and the setpoints are measured in this work using RMSE, expressed as follows:

$$RMSE = \sqrt{\frac{\Sigma(Y - Y_{set})^2}{N}} \tag{9}$$

where Y are actual values, Y_{set} are targeted values, and N is the number of samples. The RMSE decreased from 1.85 to 1.53% after the new *PID* gains were used. The new controller design caused the throttle valve to approach much closer to the setpoint in real driving conditions. The position setpoint lag of the throttle valve decreased. Consequently, the engine can respond promptly to the driver's request.

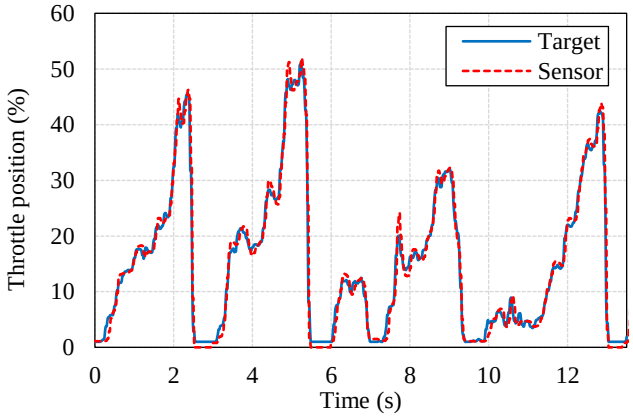

Figure 21. Throttle body position response of tuning parameters; proportional gain *P*, integral gain *I*, and derivative gain *D*, were 4, 0.137, and 30, respectively, on a proving ground

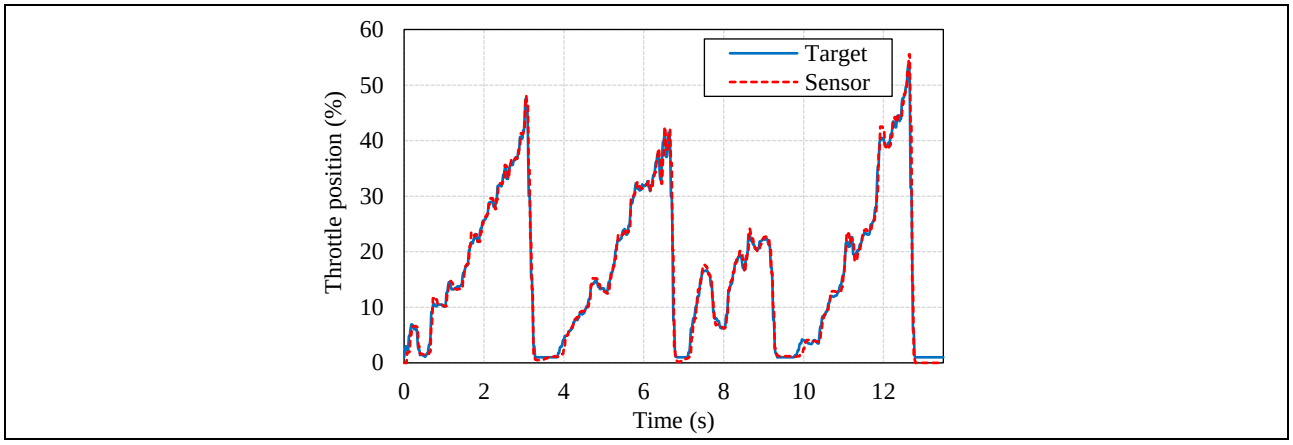

Figure 22. Throttle body position response of tuning parameters; proportional gain *P*, integral gain *I*, and derivative gain *D* were 5.5, 0.137, and 40, respectively, on a proving ground

5.0 DISCUSSIONS

i. Frequency analysis and spectrum

Frequency response analysis and spectrum analysis are powerful tools, revealing insight into the behavior of the throttle valve. Furthermore, the open-loop transfer function of the plant under consideration can be obtained by further inspecting the results of the frequency response analysis. However, this is not the case here since the ETC system is an off-the-shelf product, manufactured to work in a closed loop. Consequently, this method is unsuitable for approximating a transfer function for *PID* tuning.

ii. Electric throttle body modeling

Computer modeling provides the perspective of a *PID* controller design before implementing fine-tuning on a plant under investigation. Parameter identification helps attain a transfer function that accurately explains plant behaviors. It also reveals information about the studied plant such as nonlinearity owing to a return spring in the electric throttle body. However, this method is only helpful in providing knowledge of the transfer functions of a controller and other electronic devices of the ETC.

iii. PID tuning

The Ziegler-Nichols second method for a *PID* controller design guides the attainment of *PID* gains. Fine-tuning must then be adapted for specific plant behaviors.

In *PID* tuning, a proportional gain is initially increased so that the plant promptly responds with an acceptable overshoot. A derivative gain is subsequently added to reduce overshoot and response time. Finally, a small amount of an integral gain is added to improve steady-state error. This *PID* tuning guidance is effective and only requires knowledge concerning the principles of engineering control.

iv. Vehicle test

The formula student car with the new ETC design was tested on a proving ground, including some low-speed corners, short-straight sections, and a slalom. This study utilized RMSE to measure the magnitude deviation in the throttle valve positions from the setpoints. This quantitative parameter revealed that the position lag of the throttle valve decreased; thus, the engine responded more promptly to the driver's request.

6.0 CONCLUSIONS

This work presents an investigation of ECU behavior and provides ECU tuning guidance to improve the responses of the electronic throttle valve control system used in the formula student car. The following conclusions can be drawn:

a) The frequency response analysis was a powerful tool that revealed insight into the behavior of the throttle valve, as well as an approximated throttle valve transfer function,

b) Computer modeling provided a perspective of a *PID* controller design before carrying out fine-tuning on a plant under investigation,

c) Parameter identification made it possible to attain the transfer function presenting the plant behavior, gain additional data on the studied plant such as a nonlinearity of the return spring in the electric throttle body, and perform a preliminary *PID* selection before fine-tuning; and

d) The Ziegler-Nichols second method and fine-tuning for the *PID* controller design is most suitable, providing knowledge of the exact transfer function of the studied plant is partially available. In this study, the overshoot, the steady-state error, and the settling time of the ETC system were reduced from 29.6%, 2%, and 0.35 s to 19.33%, 0.22%, and 0.2 s, respectively. As a result, the throttle position follows the setpoint even more closely since the RMSE of the throttle position decreased from 1.85 to 1.53%.

7.0 ACKNOWLEDGEMENT

The authors would like to thank the Graduate School and Faculty of Engineering, Prince of Songkhla University for the scholarship, software licensing, and research funding.

8.0 REFERENCES

[1] N. S. Mustafa, N. H. Akhmal, M. A. Abas and M. Y. Noordin, "Application of box-Behnken analysis on the optimisation of air intake system for a naturally aspirated engine," *International Journal of Automotive and Mechanical Engineering*, vol. 17, no. 2, pp. 8029-8042, 2020.

[2] K. I. Hamada, M. F. A. Rahim, M. M. Raham and R. A. Bakar, "Throttling effect on the performance and emissions of a multi-cylinder gasoline fuelled spark ignition engine," *International Journal of Automotive and Mechanical Engineering*, vol. 19, no. 4, pp. 10084-10093, 2022.

[3] A. A. Dahlan, M. F. Muhamad Said, Z. A. Latiff, M. R. Mohd Perang, S. A. Abu Bakar and R. I. Abdul Jalal, "Acoustic study of an air intake system of SI engine using 1-dimensional approach," *International Journal of Automotive and Mechanical Engineering*, vol. 16, no. 1, pp. 6281 - 6300, 2019.

[4] M. N. Lawal, M. S. Abolarin, A. Nasir and A. N. Musa, "Differential air/fresh charge demand, supply and utilisation in two-stroke spark ignition engines," *International Journal of Automotive and Mechanical Engineering*, vol. 14, no. 4, pp. 4769 - 4784, 2017.

[5] M. A. Abd Halim, N. A. R. Nik Mohd, M. N. Mohd Nasir and M. N. Dahalan, "Experimental and numerical analysis of a motorcycle air intake system aerodynamics and performance," *International Journal of Automotive and Mechanical Engineering*, vol. 17, no. 1, pp. 7607-7617, 2020.

[6] A. S. Dewi, Z. Arifin and A. I.W., "Study case ratio gear of stepper motor on electronic throttle using PID control," *Journal of Engineering and Applied Technology*, vol. 2, no. 1, pp. 36-42, 2021.

[7] J. Kreß, J. Rau, H. Hebert, F. Perez-Pe˜na and A. M.-E. Karsten Schmidt, "Low-cost throttle-by-wire-system architecture for two-wheeler vehicles," *arXiv preprint arXiv:2304.14875*, 2023.

[8] A. J. Humaidi and A. H. Hameed, "Design and comparative study of advanced adaptive control schemes for position control of electronic throttle valve," *Information*, vol. 10, no. 2, 2019.

[9] Y. Hu and H. Wang, "Robust tracking control for vehicle electronic throttle using adaptive dynamic sliding mode and extended state observer," *Mechanical Systems and Signal Processing*, vol. 135, p. 106375, 2020.

[10] S. Jian-min and Z. Peng-tao, "Immune feedback strategy in an Electronic Throttle Control System," *Journal of Highway and Transportation Research and Development*, vol. 13, no. 3, pp. 103-110, 2019.

[11] C. Ramesh Kumar, S. Denis Ashok and B. Ashok, "Trends and future perspectives of electronic throttle control system in a spark ignition engine," *Annual Reviews in Control*, vol. 44, no. 1367-5788, pp. 97-115, 2017.

[12] M. Mcharek, T. Azib, M. Hammadi, C. Larouci and J.-Y. Choley, "Multiphysical design approach for Automotive Electronic Throttle Body," *IEEE Transactions on Industrial Electronics*, vol. 67, no. 8, pp. 6752-6761, 2020.

[13] H. Olsson, K. J. Åström, C. Canudas-de-Wit, M. Gäfvert and P. Lischinsky, "Friction models and friction compensation," *European Journal of Control*, vol. 4, no. 3, pp. 176-195, 1998.

[14] C. Canudas-de-Wit, H. Olsson, K. J. Astrom and P. Lischinsky, "A new model for control of systems with friction," *IEEE Transactions on Automatic Control*, vol. 40, no. 3, pp. 419-425, 1995.

[15] R. N. K. Loh, T. Pornthanomwong, J. S. Pyko, A. Lee and M. N. Karsiti, "Modeling, parameters identification, and control of an Electronic Throttle Control (ETC) System," in *2007 International Conference on Intelligent and Advanced Systems*, *IEEE*, pp. 1029-1035, 2007.

[16] R. Loh, W. Thanom, J. S. Pyko and A. Lee, "Electronic Throttle Control System: Modeling, identification and model-based control designs," *Engineering*, vol. 5, no. 7, pp. 587-600, 2013.

[17] "Formula SAE Rules 2023," 7 November 2022. [Online]. Available: https://www.fsaeonline.com/cdsweb/gen/-DocumentResources.aspx. [Accessed 23 January 2023].

[18] T. Ibaraki, H. Miyata, T. Uchida, M. Takada and N. Kushi, "Development of an electronic throttle control system," *JSAE Review*, vol. 15, no. 4, pp. 345-347, 1994.

[19] L. Dengfeng, B. Yunting, W. Keli and L. Yingjun, "Research on Electronic Throttle Performance Test System," in *2010 International Conference on Digital Manufacturing & Automation*, *IEEE*, vol. 2, pp. 208-211, 2010.

[20] R. Grepl, "Modelling, identification and control of electronic throttle using dspace tools," *Dynamics*, vol. 10, p. 1, 2008.